Fluid flow through ramified structures

M. P. Almeida,[1] J. S. Andrade, Jr.,[1,2,3] S. V. Buldyrev,[2] F. S. A. Cavalcante,[1,4] H. E. Stanley,[2] and B. Suki[5]

[1]*Departamento de Física, Universidade Federal do Ceará, 60455-760 Fortaleza, Ceará, Brazil*

[2]*Center for Polymer Studies and Department of Physics, Boston University, Boston, Massachusetts 02215*

[3]*PMMH-ESPCI, 10 rue Vauquelin, 75231 Paris Cedex 05, France*

[4]*Departamento de Física e Química, Universidade Estadual do Ceará, Avenida Paranjana, Fortaleza, Ceará, Brazil*

[5]*Department of Biomedical Engineering, Boston University, Boston, Massachusetts 02215*

(Received 2 March 1999)

We investigate the fluid flow through two-dimensional ramified structures by direct simulation of the Navier-Stokes equations. We show that for trees with n generations, the flow distribution strongly depends on the Reynolds number Re. Specifically, for a tree without loops the flow becomes highly heterogeneous at high Re. For a tree with loops, on the other hand, the flow distribution tends to be more uniform at increased Re conditions. We show that these apparently contradictory behaviors have the same origin, namely, the effect of inertia on the momentum transport in the channels of the ramified geometry. In order to simulate the propagation of the flow imbalance throughout the tree without loops, we develop a simple model that incorporates the basic fluid dynamics features of the system. For large trees, the results of the model indicate that the distribution of flow at the outlet branches can be described by a self-affine landscape. Finally, we argue that the nonuniform partitioning of flow found for the structure without loops may contribute to the morphogenesis and functioning of the bronchial tree. [S1063-651X(99)18210-2]

PACS number(s): 47.60.+i, 87.19.Uv

I. INTRODUCTION

The problem of fluid flow in branching geometries arises when studying a variety of phenomena in physics, geology, and biology. Examples range from fluid flow through porous media [1], a problem that has important implications for catalysis and oil recovery, to respiration [2] and blood circulation [3], where the mechanism of flow bifurcation plays a crucial role. The simplest approach to this problem consists of emulating the channels available for flow with a set of equivalent impedance elements. Such an approximation assumes a linear relation between the flux and the pressure gradient along the channels. Calculations based on linear impedance models are abundant in physics and physiological problems regardless of their limitation in reproducing some realistic details. For instance, when applied to steady or periodic flow through symmetric airway bifurcations, these models predict a perfectly homogeneous and synchronous flow distribution [4]. A network of bifurcating and merging channels is a simple model of porous media. The fluid flow through such a structure can also be mimicked by the distribution of electrical currents in a network of resistors. However, this analogy cannot account for the combined effects of fluid inertia together with the geometry of the pore space. Recently, it has been shown that, in the context of fluid flow through porous media, the linear approximation based on viscous flow conditions (Stokes' flow) is not capable of describing some crucial aspects of the phenomenon, such as the role of ''stagnant'' zones and the relevance of flow separation effects and inertia [5]. Numerical and experimental evidence presented in [6–14], support the idea that the nonlinear effects arising from the contribution of inertial forces on the transport of momentum can also have a strong influence on the properties of flow through branched structures.

With regard to physiological implications, Wilquem and

Degrez [7] investigated numerically the steady inspiratory flow through two-dimensional airway models with three generations of branches. They were able to confirm previous experimental observations [8,13] revealing a significant imbalance in the flow distribution between the medial and lateral branches of the tree. Zhao *et al.* [15] studied, both numerically and experimentally, the steady inspiratory and expiratory flow in a three-dimensional airway system of single symmetric bifurcations. They showed that the flow results obtained from computational simulations are in good agreement with the experiments, especially during expiration. In the present study, we address the question of flow asymmetry in a large network of bifurcating segments and in the presence of loops.

We investigate fluid flow through channel networks with two different types of geometries. The first is a tree of up to five generations of branches, with no loops. The second is a tree of up to nine generations of identical channels that form a subset of a hexagonal lattice. For the first type of geometry, we show that, in spite of the symmetry of the structure, the flow distribution in the last generation segments becomes highly heterogeneous at high Reynolds numbers. For the tree with loops, we demonstrate that the profile of outflow fluxes at low values of the Reynolds number can be adequately represented by the distribution of electrical currents exiting an analog resistor network model. We also observe that the flow at the outlet sections depends on the velocity at the inlet and tends to become more homogeneous as the Reynolds number is increased. The organization of the paper is as follows. In Sec. II, we present the characteristics of the numerical model and related parameters. The results are then presented and discussed in Sec. III where we also develop a binary model to represent fluid flow in this type of geometry. The results for a tree with loops are shown in Sec. IV and the

concluding considerations are presented in Sec. V.

II. MATHEMATICAL MODEL AND NUMERICAL SOLUTION

The mathematical description for the detailed fluid mechanics in a branching cascade of two-dimensional channels is based on the steady state form of the Navier-Stokes and continuity equations [16] for momentum and mass conservation, respectively,

$$\rho\left[u\frac{\partial u}{\partial x}+v\frac{\partial u}{\partial y}\right]=-\frac{\partial p}{\partial x}+\mu\left[\frac{\partial^2 u}{\partial x^2}+\frac{\partial^2 u}{\partial y^2}\right], \quad (1)$$

$$\rho\left[u\frac{\partial v}{\partial x}+v\frac{\partial v}{\partial y}\right]=-\frac{\partial p}{\partial y}+\mu\left[\frac{\partial^2 v}{\partial x^2}+\frac{\partial^2 v}{\partial y^2}\right], \quad (2)$$

$$\frac{\partial u}{\partial x}+\frac{\partial v}{\partial y}=0. \quad (3)$$

Here, the independent variables x and y denote the position in the tree, u and v are the components of the velocity vector in the x and y directions, respectively, and p is the local pressure in the system. The relevant physical properties of the flowing system are the density ρ and the viscosity μ of the fluid. In our simulations, we use air as the fluid ($\rho=1.225$ kg m^{-3}, $\mu=1.7894\times10^{-5}$ kg m^{-1} s^{-1}) and consider nonslip boundary conditions at the entire solid fluid interface. In addition, a uniform velocity profile is assumed at the inlet of the first generation channel whereas at the exits of the last generation branches, the changes in velocity rates are assumed to be zero (gradientless boundary conditions). The Reynolds number is defined as $\mathrm{Re}\equiv\rho Vd/\mu$, where d is a characteristic length chosen to be the width of the first generation channel and V is the inlet velocity. The numerical solution of Eqs. (1)–(3) for the velocity and pressure fields in the ramified structure is obtained through discretization by means of the control volume finite difference technique. The complex geometries involved in the tree of channels makes the creation of structured grids comprising quadrilateral elements very difficult, if not prohibitive. To overcome this problem, we use an unstructured mesh (see Fig. 1) based on triangular grid elements of a Delaunay network [17]. For example, in the case of a five generation tree without loops, a total of 17 864 cells generates satisfactory results when compared with numerical meshes of small resolution (differences are smaller than 1% in the outlet mass fluxes). The integral form of the governing equations (1)–(3) is then considered at each triangular element of the numerical grid to produce a set of coupled nonlinear algebraic equations which are pseudolinearized and solved using the SIMPLE algorithm [18]. For nonlinear problems which are strongly influenced by boundary conditions, the stability and convergence characteristics of a numerical method are difficult to demonstrate. In spite of this, both properties have been exhaustively checked for our computational simulations. These tests have been performed through numerical experiments before using a given solution in our study. The criteria for convergence that we used in the simulations is defined in terms of the ''residuals'' which provide a measure of the degree to which
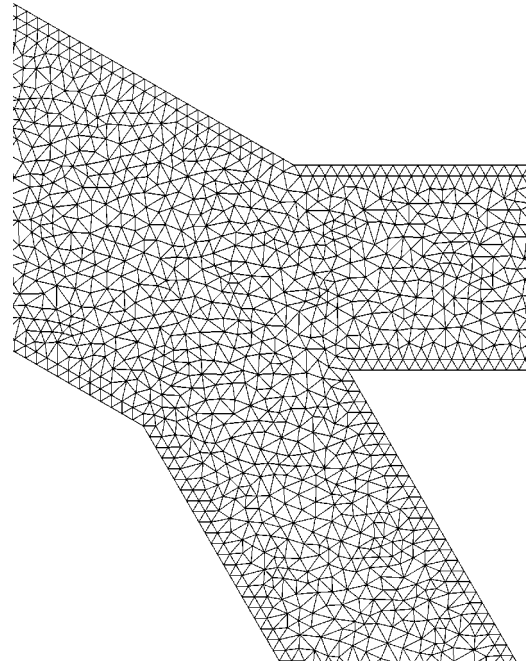

FIG. 1. Subset of the computational mesh composed of triangular elements used to solve the Navier-Stokes and continuity equations in a tree without loops.

each of the conservation equations is satisfied throughout the flow field. Residuals are computed by summing the imbalance in each equation for all cells in the domain. The residuals for each flow variable (e.g., velocity, pressure, etc.) give a measure of the error magnitude in the solution at each iteration. In general, a solution can be considered well converged if the normalized residuals are on the order of 10^{-3}. In all simulations we performed, convergence is considered to be achieved only when each of the normalized residuals fall below 10^{-3}. For a given resolution of the numerical mesh, we usually perform an additional 100 iterations to test the stability of the converged solution. A typical profile of the residuals versus iteration number for a converged solution is shown in Fig. 2. Finally, it is worth mentioning that becauseof the nonlinearity of the equation set being solved, it
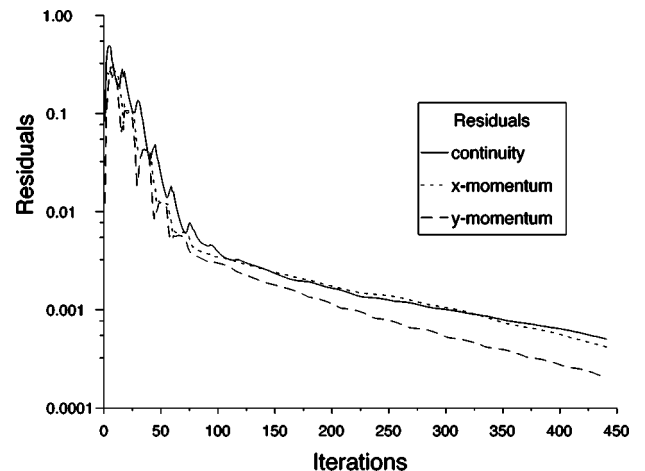

FIG. 2. Typical convergence profile obtained from our numerical simulations. Since the residuals are still decreasing after convergence is achieved, we can consider the solution to be stable.

is not generally possible to obtain a solution by fully substituting the improved values for each variable which have been generated by the approximate solution of the finite difference equation. Convergence can still be achieved, however, by *under-relaxation* which reduces the change in each variable produced during each iteration. Especially for conditions of the high Reynolds number, a large number of iterations (more than 3000 steps) is needed due to the very low under-relaxation parameters that are necessary to ensure convergence.

III. TREE WITHOUT LOOPS

The geometrical model for the tree without loops consists of a two-dimensional symmetrical cascade of rectangular channels branching along n generations of bifurcations ($n \geq 3$). In most of the simulations, we use a fixed bifurcation angle θ between daughter branches in all generations as well as realistic physiological dimensions from lung morphology [19]. Due to the symmetry with respect to the axis of the first generation channel, the flow field in only half of the domain needs to be calculated. The flow distribution in two-dimensional incompressible systems can be conveniently described in terms of the stream function, ψ which is usually defined as $u \equiv \partial \psi / \partial y$ and $v \equiv -\partial \psi / \partial x$. Figure 3(a) shows the contour plot of the stream function in a three generation tree with branching angle $\theta = 60°$ and Re=100. The lengths and widths of the channels correspond to the lengths and diameters of generations 3–5 in the morphological model of the bronchial tree proposed by Horsfield *et al.* [19]. As expected, the streamlines are equally distributed among the channels at low Reynolds conditions. As a consequence, we observe identical mass fluxes at the outlets of the terminal branches [terminals 0–3 in Fig. 3(a)]. In this situation of viscous flow, the system displays a linear behavior which validates the analogy between fluid flow in a cascade of branches and electrical transport in a network of ideal resistors [1]. At high Re values, however, the nonlinear contribution from the convective terms in Eqs. (1) and (2) becomes relevant. The effect of inertial forces on the flow field is to produce an uneven distribution of outlet fluxes in the tree [see Fig. 3(b)]. By visual inspection of the flow pattern, we note that the flux partitioning between pairs of daughter branches in the last generation [terminals 0 and 1 and terminals 2 and 3 in Fig. 3(b)] favors the branches which are aligned (1 and 2) with the inlet channel at the first generation. Figure 4 shows a closeup plot of the velocity vectors through a three generation tree calculated at Re=1200. Due to symmetry, the mass flux in the first branch (A in Fig. 4) is equally divided between the branches B (to the left) and C (to the right) composing the second generation of channels. However, the velocity profiles at the beginning of these branches are asymmetric with velocity peaks which are significantly shifted towards the inner walls (the walls close to the axis of branch A). If the lengths of segments B and C are not too large and Re is sufficiently high, the flow still displays an asymmetric profile at the distal ends of channels B and C. As a consequence, the fluxes entering the next generation daughter branches (D and E of branch B and F and G of branch C) are different: the fluxes entering the inner branches (E and F that are aligned with branch A) are higher
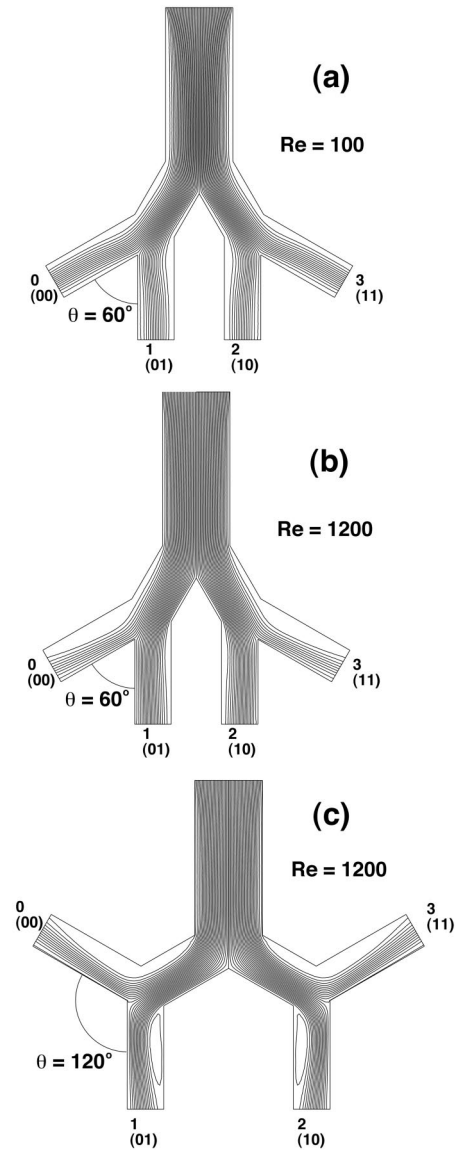

FIG. 3. (a) Contour plot of the stream function in a three generation tree with bifurcation angle $\theta = 60°$ and Re=100. Fluid is pushed from top to bottom throughout the tree. Also shown is the binary representation of each outlet branch. (b) Same as in (a) but for a higher Reynolds number (Re=1200). (c) Same as in (b) but for $\theta = 120°$. The larger the number of streamlines in a branching element, the higher the flux. Note that the streamlines are equally distributed among the last generation channels in (a), while in (b) and (c) the outlets 1 and 2 have higher fluxes compared to outlets 0 and 3. Also, the number of streamlines and thus the fluxes at outlets 1 and 2 are larger in (b) than in (c).

than those entering the outer branches (D and G). When the branches are sufficiently long and/or the Reynolds number is low, a symmetric shape of the velocity profile at the exits of branches B and C can be reestablished by viscous forces. In this situation, the mass fluxes in B and C split into equal amounts at the bifurcation sections, maintaining, therefore, the symmetry of the flow distribution. We examine the contribution of inertia to the flow nonuniformity by computing the flow rates at the eight exits on the left-hand side of a five generation tree. As shown in Fig. 5, at high Re, the local
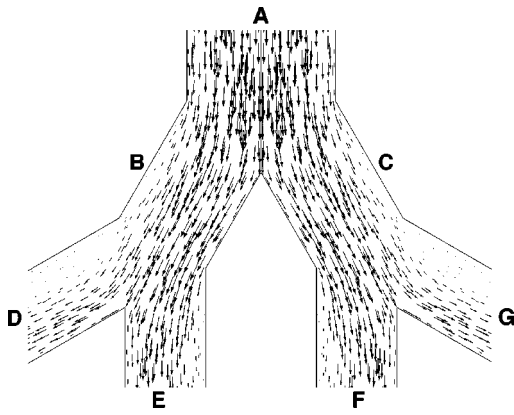
FIG. 4. Closeup of the velocity vector field in the first three generations of channels comprising a tree without loops (Re $=1200$). The effect of inertia on the fluid flow is revealed by the asymmetric distribution of velocity vectors in branches B and C. Vectors with large magnitudes are substantially shifted toward the direction of the axis of channel A. The propagation of this effect throughout the remaining generations is responsible for the flux heterogeneity at the outlets of the flowing system at high Re conditions.

flow partitioning between any two daughter branches (branches that belong to the same parent) favors the branch which is aligned with the grandparent branch (branch located two generations above in the same cascade). Following the enumeration scheme presented in Fig. 5, Fig. 6 shows how the outlet fluxes normalized by the total flux penetrating the system (through the first generation channel) become progressively more heterogeneous as Re increases from 150 to 4800. As can be seen, the normalized flow rates at exits 5 and 10 are substantially increased compared to those at the other exits when the convective mechanism of momentum transport becomes a dominating mechanism in determining the fluid flow field. The branching angle θ has a strong influence on the distribution of flows. A comparison between the contour plots shown in Figs. 3(b) and 3(c) clearly indicates that for high Re the tendency in which the flow favors the internal branches is greatly enhanced for a tree with a
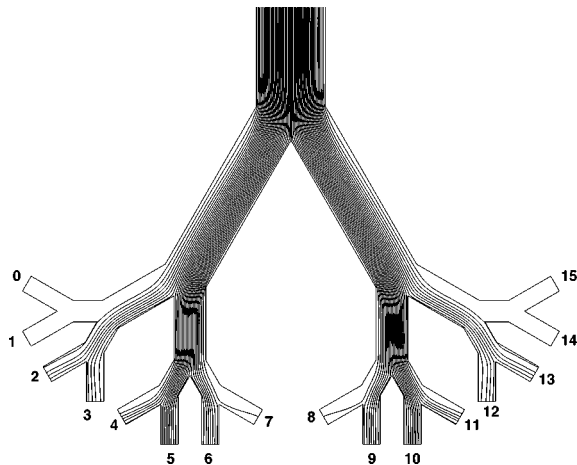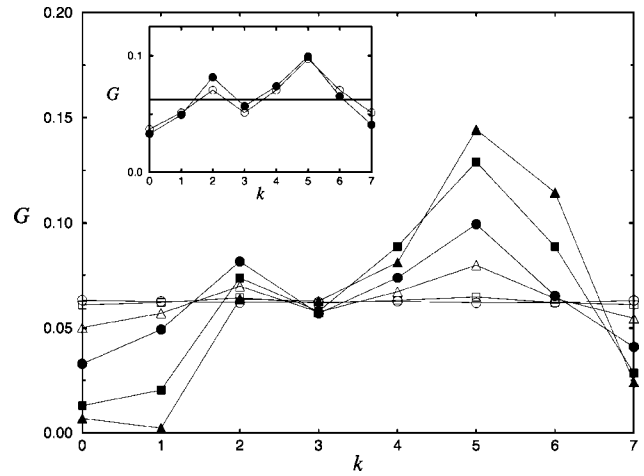

FIG. 6. Flux distributions G at the outlet branches in a five generation tree for Re$=150$ (circle), 300 (square), 600 (triangle), 1200 (full circle), 2400 (full square), and 4800 (full triangle). The inset compares the fluid flow simulations (Re$=1200$, circle) and the binary tree model ($p=0.58$, full circle).

smaller branching angle. This observation is quantified in Fig. 7, where we show, for two different values of θ, the dependence on Re of the ratio G_1/G_0 of the fluxes at the internal (G_1) and external (G_0) outlets of the third generation branches. As expected, for a fixed branching angle, both curves show a gradual increase of G_1/G_0 with the Reynolds number. Furthermore, for high Re, the value of G_1/G_0 becomes significantly larger for $\theta=60°$ than for $\theta=120°$. In order to elucidate the effects of the branching angle θ on the asymmetry of flow, additional fluid dynamic simulations with three generation trees have been performed. We denote the branching angle between the first generation of daughter branches (B and C in Fig. 4) by θ_1 and the branching angle between the second generation of daughter branches (D and E, and F and G in Fig. 4) by θ_2. The simulations are carried out according to the following specifications. (1) The bifurcation angle θ_2 is fixed to $120°$. (2) The internal exit branches (branches E and F in Fig. 4) are kept aligned with the root (branch A) independently of θ_1 (the bifurcation

FIG. 5. Contour plot of the stream function in a five generation tree without loops for high Reynolds number conditions (Re $=4800$). The width of the first channel is $d=1.8$ cm and the length is $l=12$ cm.
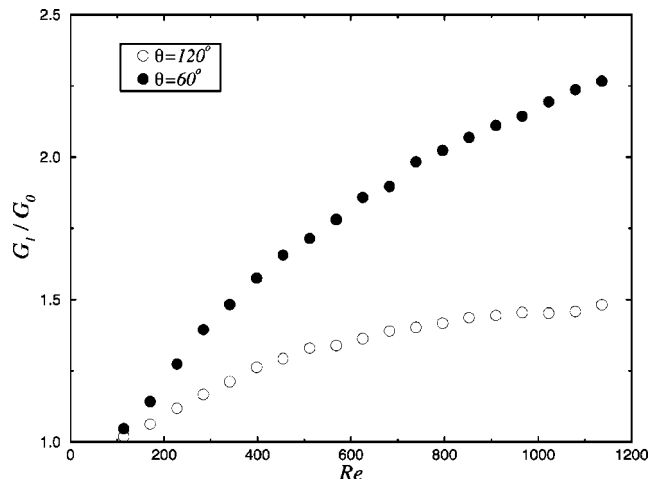

FIG. 7. Dependence of the flux ratio G_1/G_0 on the Reynolds number Re in three generation trees for two different values of the bifurcation angle θ.
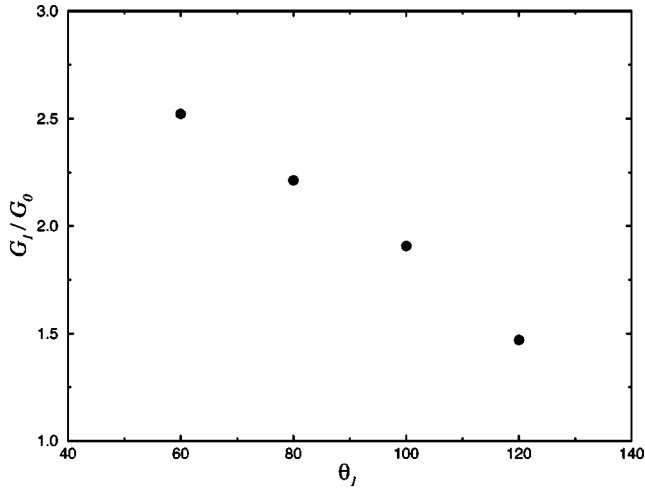
FIG. 8. Dependence of the flux ratio G_1/G_0 on the bifurcation angle θ_1 between daughter branches at the second generation. The simulations have been performed with three generation trees at high Reynolds conditions (Re$=1200$). The bifurcation angle at the second generation is $\theta_2=120°$.

FIG. 9. Dependence of the flux ratio G_1/G_0 on the pressure drop ratio $\Delta p_1/\Delta p_0$ in three generation trees ($\theta=120°$ and Re$=1200$).

angle between branches B and C). (3) We use the same Reynolds number for all simulations (Re$=1200$). Note that for Re$=1200$, the flux ratio with equal bifurcation angles ($\theta_1=\theta_2=120°$) is $G_1/G_0=1.47$ (see Fig. 7). (4) Simulations are then carried out for different values of the bifurcation angle θ_1 ($\theta_1=60°,80°,100°$, and $120°$).

In Fig. 8, we clearly see that increasing the angle θ_1 from $\theta_1=60°$ to $\theta_1=120°$ results in a decrease of the flux ratio G_1/G_0 from 2.52 to 1.47, respectively. Based on these and the previous simulations, we conclude that there are two geometrical factors to be considered when analyzing the branching angle effect on the flux partitioning.

(i) If we keep the internal exit branches (branches E and F in Fig. 4) aligned with the root, a large branching angle between outlets 0 and 1 will correspond to a high flux ratio G_1/G_0. This effect is solely due to the relative alignment of the outlets (third generation branches) with the inlet branch.

(ii) The second factor refers to the horizontal shift between the inlet and internal outlet branches caused by the first branching angle θ_1. That is, while the outlet branches and the root remain parallel (E and A, and F and A), for a larger θ_1 the horizontal distance between branches E and A (and F and A) increases. This shift reduces the flux ratio considerably and is responsible for the lower flux ratio at higher branching angles.

Thus, for a given fixed Re, when θ_1 and θ_2 increase together as in Fig. 7, due to the increased horizontal distance between the root (branch A) and the internal outlet branches (E and F), the flux partitioning decreases. Finally, we perform a series of simulations with a tree of three generations and branching angles of $120°$ to demonstrate that the asymmetry effect caused by inertia is rather robust against the outlet pressure boundary conditions. A constant flow rate is imposed at the inlet of the system (Re$=1200$) and we gradually change the pressure at the end of the internal branches [outlets 1 and 2 in Fig. 3(a)] keeping the static (gauge) pressures of the external branches [outlets 0 and 3 in Fig. 3(a)] constant (equal to zero, for reference). Obviously, since the flow rate is fixed at the inlet, the pressure at the inlet will
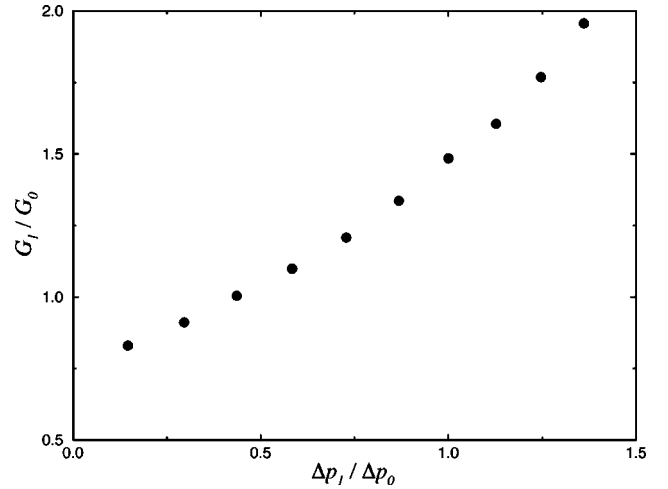
change when the pressure at any of the exits is modified. We therefore calculate the average pressure at the inlet by integrating over all fluid cells connected with the interface. The results of these simulations are displayed in Fig. 9 where we show the dependence of the mass flux ratio G_1/G_0 on the ratio between the pressure drops of outlets 1 (Δp_1) and 0 (Δp_0) in relation to the static pressure at the inlet of the first generation channel. For a ratio $\Delta p_1/\Delta p_0$ of unity, we recover the flux ratio ($G_1/G_0=1.47$) found for Re$=1200$ and $\theta=120°$ (see Fig. 7). More importantly, we observe that in order to reestablish a ''symmetric'' flux partitioning ($G_1/G_0=1$) one has to apply $\Delta p_1/\Delta p_0\approx0.43$. Thus, a strong asymmetry of the outlet pressures (variability $>100\%$) is necessary in order to compensate for the flux asymmetry due to inertial effects at high Reynolds numbers.

A. Binary model

All the fluid dynamic features presented in the preceding section can be combined in a model to qualitatively describe the role of convection on transport of fluid in a self-similar branching system of two-dimensional channels. First, we assume that every branch of the next generation forms an angle of $\pm\theta$ degrees with its parent. Also, we assume that the Reynolds number is sufficiently high at the entrance so that it is also high at each bifurcation. As a consequence, the flux partitioning can be taken to be approximately constant and independent of the Reynolds number (see Fig. 7). Thus, we assume that the flux partitioning is constant throughout the tree so that the flow rates in any two daughter branches divide always in a fixed proportion of p/q, where $p+q=1$, $p>q$, and $p=f(\text{Re},\theta)$. The effects of convective momentum transport are then mimicked by assigning the larger factor p to the flow of the daughter branch which is aligned with its grandparent. All branches in generation n are numbered from 0 to $2^{n-1}-1$. In this way, the branch k in generation $n-1$ bifurcates to branches $2k$ and $2k+1$ in generation n. The branch $2k$ forms an angle $-\theta$ and the branch $2k+1$ forms an angle $+\theta$ with the parent. Following this scheme, the branch $2k+1$ (odd) is aligned with its grandparent if k is even and the branch $2k$ (even) is aligned with its
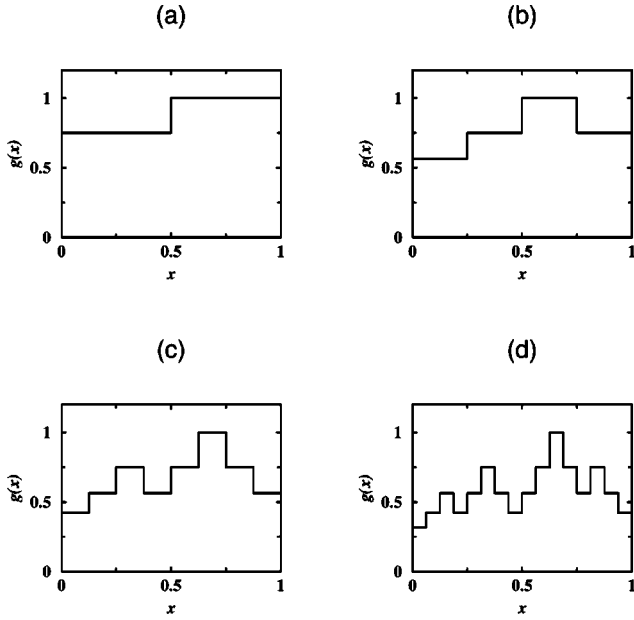
FIG. 10. Construction of the self-affine landscape of normalized fluxes $g(x)$ defined in Eq. (5) as a function of the normalized branch number. Successive applications of Eq. (6) using the steplike function $g_3(x)$ shown in (a) generates (b) $g_4(x)$, (c) $g_5(x)$, and (d) $g_6(x)$.
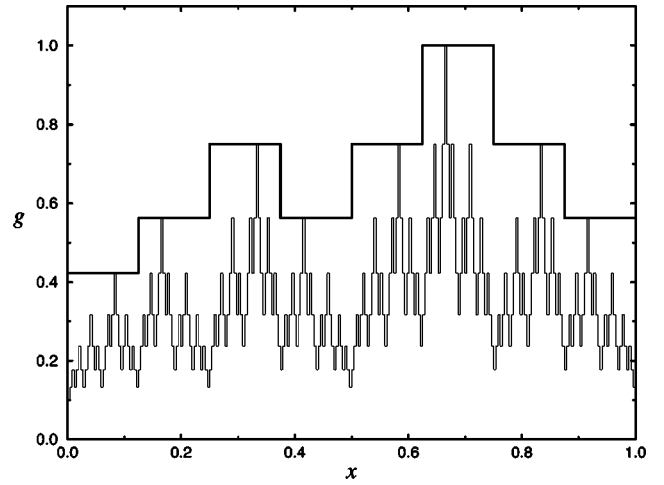

FIG. 11. Distribution of normalized fluxes $g(x)$ defined in Eq. (5) as a function of the normalized branch number x at the outlets of a five generation (thick line) and a ten generation (thin line) tree. These steplike functions are calculated using the binary tree model with a partitioning ratio $q/p = 0.75$.

grandparent if k is odd. As a consequence, a branch will be aligned with its grandparent if the two last digits in its binary representation are different. For a tree of three generations, the branches should have flows as $q/2$, $p/2$, $p/2$, $q/2$, corresponding to their binary codes 00, 01, 10, and 11, respectively. By induction, for a tree with n generations, the flow in branch k should then be

$$G(n,k) = \frac{1}{2} p^{l(k)} q^{n-2-l(k)}, \tag{4}$$

where $l(k)$ is the number of *switches* from 1 to 0 and from 0 to 1 in the binary representation of k with $n-1$ digits. For instance, in a tree of five generations, the branches with numbers 5 and 10 will have the maximum flow of $p^3/2$ because their binary representations, 0101 and 1010, respectively, both have 3 *switches*. This simple binary model predicts a flux distribution that is compatible with the direct solution of the Navier-Stokes equations (see Fig. 6 inset). Due to the symmetry of the tree, we only need to analyze the flow distribution through its first half. Thus, for generation n, we can normalize the flow G in branch k by the factor $p^{n-2}/2$ and define the steplike flux function,

$$g_n(x) = \left(\frac{q}{p}\right)^{n-2-l(k)} \tag{5}$$

for $k/2^{n-2} \leq x < (k+1)/2^{n-2}$ with $k = 0,1,\ldots,(2^{n-2}-1)$. In this way, for $n \geq 3$ and $x \in [0,1)$, $g_n(x)$ is a well defined right-continuous and positive function with an upper bound of 1. The four first functions of this series (g_3,g_4,g_5, and g_6) are shown in Fig. 10. The function g_n has 2^{n-2} steps which are sequentially numbered beginning from 0. We observe that g_{n+1} can be generated from g_n if we simply mul-

tiply $g_n(x)$ by a scaled g_3 if k is even or multiply $g_n(x)$ by a scaled mirror of g_3 if k is odd, i.e.,

$$g_{n+1}(x) = \begin{cases} g_n(x)g_3(2^{n-2}x-k) & \text{if } k \text{ is even,} \\ g_n(x)g_3(k+1-2^{n-2}x) & \text{if } k \text{ is odd.} \end{cases} \tag{6}$$

For a fixed $x \in [0,1)$, the sequence of numbers $g_n(x)$ resulting from this iterative process, $n=3,4,\ldots$ converges to a value $g(x) \in [0,1]$. Therefore, we can define the function

$$g(x) = \lim_{n \to \infty} g_n(x) \quad x \in [0,1), \tag{7}$$

which is also non-negative, bounded by 1 and everywhere discontinuous in the interval $[0,1)$. For instance, the maximum flow $g^{max} = 1$ will be located at $x = 2/3$ since its binary representation is $0.1010101\ldots$ which has the maximum possible number of *switches* in the sequence. In the limit $n \to \infty$, $g(x)$ is equal to 0 for every x except values of x which are periodic (with period 01) in their binary representation. For all the other numbers $k-2-s(k) \to \infty$ as $n \to \infty$, and hence $g(x) \to 0$. It can be readily shown that the following identity is also valid in the limit $n \to \infty$:

$$g(x) = \left(\frac{q}{p}\right)^m g(2^m x) \quad \text{for} \quad 0 \leq x < \frac{1}{2^m}. \tag{8}$$

This relationship (8) indicates that the landscape (see Fig. 11) generated from the fluxes at the exits of the ramified structure is self-affine [20], i.e., $g(x) \propto b^{-\alpha} g(bx)$, with an exponent $\alpha = \log_{10}(p/q)/\log_{10}2$. If $2^m x$ has binary representation $0.x_1 x_2 \ldots x_k 0101 \ldots$, then it is easy to show that x is represented by $0.000 \ldots x_1 x_2 \ldots x_k 0101 \ldots$ which has m switches less than the binary representation of $2^m x$. Hence, we obtain the prefactor $(q/p)^m$.
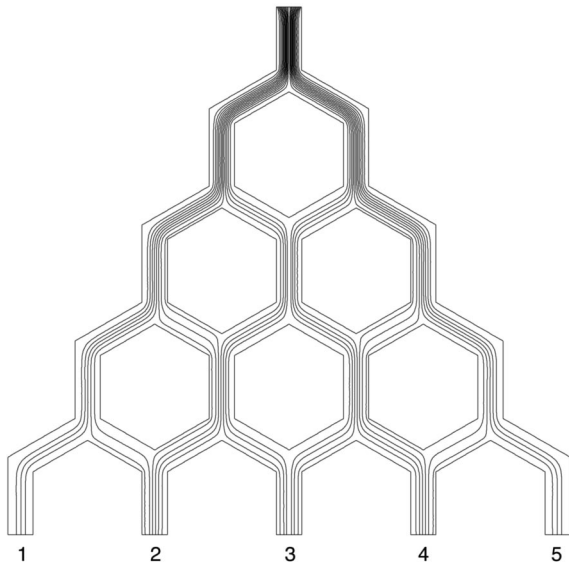
FIG. 12. Contour plot of the stream function in a five generation tree with loops. In this case, fluid is pushed from top to bottom throughout the tree at low Reynolds conditions (Re=1). Note that the number of streamlines is larger (and thus the fluxes are higher) at the center channels in the last generation.

IV. TREE WITH LOOPS

The detailed geometry of the tree with loops adopted in the present study is analogous to a subset of a hexagonal lattice whose bonds are two-dimensional channels with equal lengths and widths (see Fig. 12). Hence, the fluid domain is essentially a sequence of closed loops of channels. Due to its geometry, the flow field in this structure has a distinct and opposite trend as compared with the flow field in a tree without loops. Figure 12 shows the contour plot of the stream function in a five generation tree at a low Reynolds conditions (Re=1). In contrast with Fig. 3(a) where we observe a uniform distribution of streamlines among branches in the same generation at low values of Re, Fig. 12 shows a higher density of streamlines in the center channels (channels which are close to the axis of the first generation channel). In Fig. 13 we show the profile of outlet mass fluxes at low Re in a nine generation tree. In the limit of low Reynolds numbers, the flux on the looped structure can also be found by solving the analog electrical circuit problem [21]. The analytic solution that gives the velocities in the looped structure when the number of generations $k \rightarrow \infty$ can be found by a conformal mapping of an equilateral triangle onto the upper semicircle in the complex plane z with two charges $\ln(z-i)$ and $-\ln(z+i)$. As shown in Fig. 13, this analytic solution is in good agreement with the flux distribution obtained from the numerical solution of the Navier-Stokes equations. At high Reynolds numbers, the flow pattern at the outlet level departs from that obtained by the electrical analog model (Fig. 14). As we gradually increase Re, the profile of outlet fluxes becomes more uniform due to a relative increase in the flows carried by the segments far from the symmetry axis of the system. In contrast to the fluid flow characteristics observed in a tree without loops, the effect of inertia here is to ''delocalize'' the velocity field so that a condition of homogeneous flow field is generated.
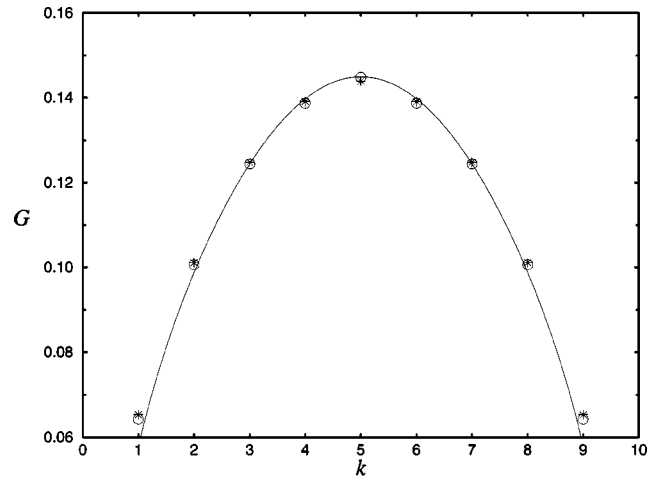

FIG. 13. Flux distribution at the outlet branches of a nine generation tree with loops for Re=1 (circle). The results from an analog electrical network model (star) are in agreement with the fluid dynamic simulations. The solid line is the analytical solution of the infinite network [21].

V. DISCUSSION

The classical correspondence between fluid flow and electrical current in analog resistor networks certainly represents a simple and useful approximation, especially when the fluid domain is a complex geometry, as in the case of trees of channels with or without loops studied in the present work. This analogy, valid only for low Reynolds numbers or, more precisely, in the situation of Stoke's flow, is consistent with the assumption that fluid flow in such complicated morphologies should not depend on the relative direction of the channels. Therefore, if Hagen-Poiseuille's flow is locally applicable, only the dimensions (width and length) of the rectangular channels composing the ramified structure should contribute to their corresponding *hydraulic conductance* σ. In this case, a change in the bifurcation angles between daughter channels in the branching cascade should have no effect on the momentum transport and continuity through the tree, a situation which is entirely analogous to the distribution of currents in an electrical resistor network. At increased
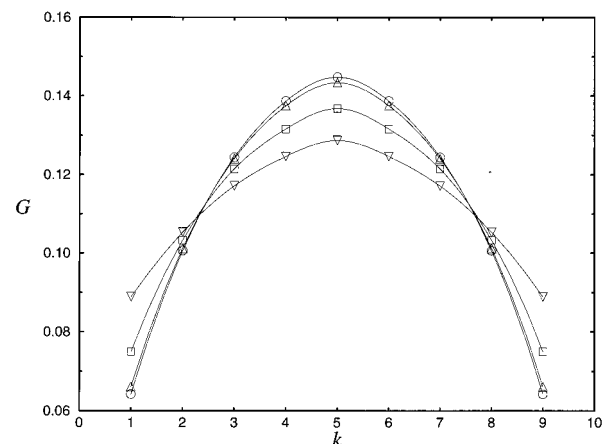

FIG. 14. Flux distribution at the outlet branches of a nine generation tree with loops for Re=1 (circle), 10 (triangle up), 100 (square), and 1000 (triangle down).

Reynolds numbers, however, the convective mechanism of momentum transport becomes relevant and the changes in the relative directions of the channels (occurring at the bifurcations/curves) can significantly affect the flow pattern. More specifically, we note that the flow field in a tree without loops becomes more heterogeneous at high Reynolds numbers, as opposed to the highly uniform distribution of fluxes found for low Re flow. Interestingly, the effect of inertia on the flow through a tree with loops is to enhance the transport of momentum and then promote a more uniform distribution of streamlines among different fluid pathways. To some extent, this corresponds to a ''delocalization'' of velocity field. Thus, the presence of loops in a tree structure can have very important consequences on the established flow field.

With regard to the physiological implications of our results, we note that Fig. 4 suggests that the relative flows delivered to the various outlets of this symmetric structure become increasingly asymmetric with a large variability for large Re. Applied to steady flow conditions during inspiration, our model predicts that the amount of air and hence oxygen delivered to the periphery of the lung is also very heterogeneously distributed among the alveoli where gas exchange occurs. This appears to be in contradiction to the fact that time constant inequalities among parallel pathways are relatively small in the normal lung and hence ventilation distribution should be fairly uniform and primarily determined by the distribution of local compliances [22]. The flow heterogeneity at the outlets of the branching cascade certainly depends on the loads and their heterogeneities attached to the last generation channels. In the airway tree these loads are the compliance of the alveolar wall tissue and the compressibility of the alveolar gas. One may argue that flow asymmetry in the bronchial tree is very likely to be a consequence of the unequal pressure distribution at the lower generation branches due to heterogeneities in the compliant elements. Experimental data obtained using the alveolar capsule technique [25] provide evidence that at low frequencies (close to the breathing rate of ≈ 0.1 Hz), the coefficient of variation of alveolar pressures in phase with lung volume is between 2% and 6%. Our simulation results in Fig. 9 indicate that this amount of variability in pressures at the exits is significantly smaller than the variability necessary to eliminate the flux heterogeneity due to convective inertia. Thus, alveolar pressure nonhomogeneity in the lung cannot compensate for the large flux heterogeneity, yet ventilation distribution (fluxes delivered to the periphery) is reasonably uniform. The question therefore arises as to what are the mechanisms in the real lung that can balance flow imbalance due to nonlinear inertial effects? Below, we discuss three possible mechanisms.

First, our simulation uses a symmetric Cayley tree, whereas the geometrical structure of the airway tree is highly asymmetric. In Horsfield's airway tree models, asymmetry not only means that some branches are missing, but the diameters of the branches toward a shorter pathway decrease faster leading to smaller size subtrees [19]. Thus, one possible mechanism that may compensate for flow imbalance due to nonlinear inertial effects is structural asymmetry. In other words, the central airways receiving smaller flows (due to inertia) may serve correspondingly smaller alveolar regions that match the size of the region. This would then allow for a homogeneous ventilation distribution which is required for the normal functioning of the lung.

The second possible mechanism is related to the existence of loops in the tracheobronchial tree. These loops, called collateral airways, are channels connecting different subtrees in the tracheobronchial structure [27,23]. The primary role collateral airways may play in the functioning of the lung has been a controversial issue in the literature. Our simulations may provide a new interpretation for their physiological function. Figure 14 shows that when the Reynolds number is high, flow distribution at the outlets of the tree with loops tends to become more homogeneous. Thus, similarly to the effect of loops that compensate for the asymmetry in flow caused by inertia, the collateral airways may help in providing a more homogeneous flow delivery to the periphery and hence ventilation distribution.

Third, our simulations assume rigid channel walls. However, the airways are compliant structures in the lung. When flow is large in a segment, due to the Bernoulli effect, lateral pressure near the airway wall decreases and hence transmural pressure across the compliant wall increases. As a result, the airway diameter decreases and so does local Reynolds number. Thus, flow distribution will be altered in the nearby segments in a manner that reduces flow heterogeneity. It is also possible that the smooth muscle in the airway wall can locally regulate airway wall compliance so that flow heterogeneity and hence ventilation distribution becomes more uniform.

While the above mechanisms may act to reduce flow heterogeneity, they are not sufficient to make the flow distribution uniform. Unfortunately, large trees are impossible to treat numerically. Our binary tree model is, however, very useful as it can provide insight into the effect of inertia on the flow distribution in large trees. The self-affine structure of flow partitioning indicates a heterogeneous flow distribution; we expect that this feature does not depend on the approximations in the binary tree model, namely, constant angles and constant p along the tree. In reality, p may depend in a complex manner on the actual geometry. However, it is the mean value of p that determines flow distribution in the periphery [26]. Using three, four, and five generation trees, we find an average value of $p/q = 1.45 \pm 0.03$ which gives $p \approx 0.59$ at Re$=1200$. This value is consistent with $p=0.58$ used in the binary tree model to fit the flow data. The small variability ($\approx 6\%$ of the mean) confirms our assumption that the p/q ratio is approximately constant throughout the generations for sufficiently large Re values. The exponent α is useful in quantifying the effect of asymmetry due to flow partitioning in large trees. Using the values of p and q reported in Ref. [26], we find $\alpha = 0.9$ for the human lung and $\alpha = 1.6$ for the more asymmetric dog lung.

Finally, we note that it was argued in Ref. [24] that the asymmetric structure of the lung is solely due to geometrical constraints. Our study, however, suggests a possible different origin for this structure since the asymmetry of the bronchial tree can be influenced by the fluid flow asymmetry combined with the requirement of homogeneous ventilation.

[1] P.M. Adler, *Porous Media: Geometry and Transport* (Butterworth-Heinemann, Stoneham, MA, 1992).

[2] R. H. Ingram, Jr. and T. J. Pedley, in *Handbook of Physiology. The Respiratory System. Mechanics of Breathing* (American Physiological Society, Bethesda, 1986).

[3] D. MacDonald, *Blood Flow in Arteries* (Williams & Wilkins, Baltimore, 1974).

[4] T.J. Pedley, R.C. Schroter, and M.F. Sudlow, Respir. Physiol. **9**, 387 (1970).

[5] J.S. Andrade, Jr., M.P. Almeida, J. Mendes Filho, S. Havlin, B. Suki, and H.E. Stanley, Phys. Rev. Lett. **79**, 3901 (1997).

[6] J.S. Andrade, Jr., A.M. Alencar, M.P. Almeida, J. Mendes Filho, S.V. Buldyrev, S. Zapperi, H.E. Stanley, and B. Suki, Phys. Rev. Lett. **81**, 926 (1998).

[7] F. Wilquem and G. Degrez, J. Biomech. Eng. **119**, 59 (1997).

[8] B. Snyder, D.R. Dantzker, and M.J. Jaeger, J. Appl. Physiol.: Respir., Environ. Exercise Physiol. **51**, 598 (1981).

[9] B. Snyder and M.J. Jaeger, J. Appl. Physiol.: Respir., Environ. Exercise Physiol. **54**, 749 (1983).

[10] A.S. Slutsky, G.G. Berdine, and J.M. Drazen, J. Appl. Physiol.: Respir., Environ. Exercise Physiol. **49**, 417 (1980).

[11] D.J. Isabey, J. Biomech. **15**, 395 (1982).

[12] J.L. Allen, I.D. Frantz, and J.J. Fredberg, J. Clin. Invest. **76**, 620 (1985).

[13] A. Tsuda, and J.J. Fredberg, J. Appl. Physiol. **69**, 546 (1990); **69**, 553 (1990).

[14] I. Balaśhaźy and W. Hofmann, J. Aerosol Sci. **24**, 745 (1993).

[15] Y. Zhao, C.T. Brunskill, and B.B. Lieber, J. Biomech. Eng. **119**, 52 (1997).

[16] R.B. Bird, W.E. Stewart, and E.N. Lightfoot, *Transport Phenomena* (John Wiley & Sons, New York, 1960).

[17] D.F. Watson, Comput. J. (Switzerland) **24**, 167 (1981).

[18] S.V. Patankar, *Numerical Heat Transfer and Fluid Flow* (Hemisphere, Washington, DC, 1980). We use the FLUENT fluid dynamics analysis package (FLUENT Inc.) in this study.

[19] K. Horsfield, W. Kemp, and S. Phillips, J. Appl. Physiol.: Respir., Environ. Exercise Physiol. **52**, 21 (1982).

[20] The term *fractal* refers to the general class of objects which are invariant under scale transformations. More specifically, objects which are invariant under isotropic scale transformations are called *isotropic fractals* or *self-similar* fractals. The term *self-affine fractal* refers to the class of objects which are invariant under anisotropic scale transformations; A. L. Barabasi and H. E. Stanley, *Fractal Concepts in Surface Growth* (Cambridge University Press, Cambridge, 1995).

[21] The analytic solution which gives the velocities in the looped structure when the number of generations $k \to \infty$ can be found by a conformal mapping of an equilateral triangle onto the upper semicircle in the complex plane z with two charges $\ln(z-i)$ and $-\ln(z+i)$. If we introduce a continuous variable $x=k/n-1/2$, where $k=0,1,2,\ldots,n$ is the segment number, then the velocity $v(x)$ is given by

$$v(x) = \left[\frac{4f(1)}{3\sqrt{3}\ n \ln n} + O\left(\frac{1}{n \ln^2 n}\right) \right] \left(\frac{1-t^2(x)}{1+t^2(x)}\right)^{-1/3},$$

where $f(t)$ is a Christoffel integral

$$f(t) = \int_0^t dy [(y^2+1)^2(1-y^2)]^{1/3},$$

and $t(x)$ is a function defined as the inverse function with respect to the function $x(t)=f(t)/[2f(1)]$. The numerical value of the quantity $f(1)$ is approximately equal to 1.051 63. The total conductance decreases with generation number as

$$c = \frac{\pi}{3\sqrt{3}\ln n} + O\left(\frac{1}{\ln^2 n}\right).$$

The estimation of the coefficient for the second term in conductance is -0.205. The numerical solution of the discrete problem converges to the analytical limit in powers of a logarithm.

[22] J. MilicEmili, *The Lung: Scientific Foundations*, edited by R. G. Crystal *et al.* (Raven Press Ltd., NY, 1991).

[23] W. Mitzner (private communication); W. Mitzner, *The Lung: Scientific Foundations Second Edition*, edited by R. G. Crystal *et al.* (Lippincott-Raven Publisher, Philadelphia, 1997).

[24] T.R. Nelson and D.K. Manchester, IEEE Trans. Med. Imaging **7**, 321 (1988).

[25] B. Suki, Z. Hantos, B. Daróczy, G. Alkaysi, and S. Nagy, J. Appl. Physiol. **71**, 69 (1991).

[26] H. Kitaoka and B. Suki, J. Appl. Physiol. **82**, 968 (1997).

[27] M.W. Lambert, J. Pathol. Bacteriol. **70**, 311 (1955).